Numerical study on the influence of electron temperature on void formation in dusty plasma

Yan Wang[1], Xu Zhu[2], Zhaoyang Chen[1,4] and Feng Huang[3,4]

[1] College of Mathematics and Physics, Beijing University of Chemical Technology, Beijing 100029, People's Republic of China
[2] PVD Business Unit, Beijing NAURA Microelectronics Equipment Co., Ltd, Beijing, 100176, People's Republic of China
[3] College of Science, China Agricultural University, Beijing 100083, People's Republic of China

E-mail: chenzy@mail.buct.edu.cn and huangfeng@cau.edu.cn

CrossMark

Abstract

In the past, experiments have proven that the electron temperature in the void is lower than that in the dust cloud. Based on this point, the influence of the spatial distribution of the electron temperature on the void is studied by calculating the fluid equation with explicit ionization, and the images of the circular void and the ring void are obtained by simulation. It is found that when the electron temperature is greater than the threshold value, a stable circular void is generated, and as the electron temperature increases, the time required for the circular void to reach a steady state decreases and its size decreases. This law is not affected by electron temperature spatial distribution set in the center. Combined with the studies of circular void, we speculate that the electron temperature in the ring void is also lower than that in the dust cloud. Through the assumption of the spatial distribution of electron temperature, the simulation results in a ring-shaped void. And the influence of the intensity of the spatial variation of the electron temperature on the ring void is verified. The results show that when the electron temperature change is severe enough, a ring void is generated. And as the intensity increases, the time required for the ring void to reach a steady state decreases, and the size increases slightly.

Keywords: void, electron temperature, fluid simulation, dusty plasma

(Some figures may appear in colour only in the online journal)

1. Introduction

Dusty plasma is a plasma system containing a large number of negatively charged dust particles as well as electrons and ions. It is ubiquitous in the Universe [1]. For example, it exists in the interstellar space, solar system, the Earth's ionosphere, etc It also exists in fusion devices and appears in the semiconductor, low temperature plasmas and nanotechnology industries [1]. Research on dusty plasmas is thus relevant to space science, astrophysics, plasma chemistry, etc In the past decades, much work has been carried out on linear and nonlinear waves in the dusty plasmas (including dust-acoustic waves, dust ion-acoustic waves, dust shocks and solitons), the dust charging process, dust crystal formation, and dust voids. A void is a local dust-free region that spontaneously evolves in the dusty plasma, with sharp dust cloud boundaries [2–7]. Many experimental and numerical studies have been carried out on the evolution and development of voids. In early laboratory experiments, Selwyn and Heidenreich *et al* tracked the dust particles and their motion in real time by laser scattering in RF etching reactor, and finally observed rings of particles and domes of particles [8]. Huang *et al* obtained clear void images in the RF discharge dusty plasma system, including circular voids, ring voids, and the above two types of coexisting voids images, and the ring void appeared later than the circular void [3, 4]. Morfill *et al* also observed voids in microgravity experiment [7].

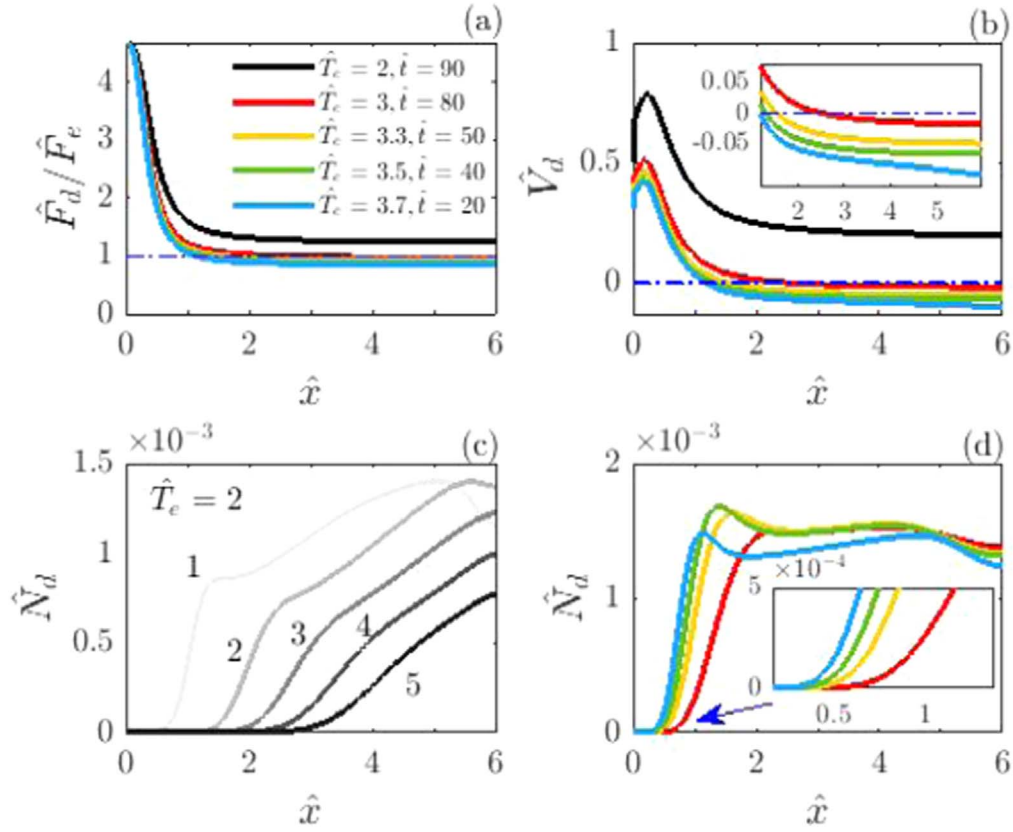[4] Authors to whom any correspondence should be addressed.

Figure 1. The spatial distribution of (a) the ratio of ion drag force to electrostatic force and (b) dust particle velocity. (c) Spatial distribution of the dust particle number density when $\hat{T}_e = 2, \hat{t} = 10, 30, 50, 70$ and 90 (corresponding to curves 1–5 in turn). (d) The spatial distribution of the dust particle number density at the steady state at different electron temperatures. The value of $\hat{t}$ given in figure 1(a) is the time to reach steady state. All the presented results presented here are at steady state. The electron temperature was set to be evenly distributed in space.

Voids exist widely in plasma processing discharges experiments, and researches related to voids have attracted much attention. The effects of different conditions such as gas pressure, discharge power, and discharge current on the generation and evolution of voids are given in [2, 9–13]. Tsytovich *et al* gave the theoretical and numerical results of the dependence between physical properties of the void and the power input into the plasma [14]. Sarkar *et al* experimentally added a ring electrode between the DC electrodes and dynamically controlled the void region by changing the positive bias voltage outside the ring electrode [15]. Shumova *et al* studied the effect of void on plasma parameters in discharge with voids in dust structures [16]. The stability of dust void was also studied in [17–19]. Tsytovich *et al* discussed the effect of ion diffusion on neutral gas atoms on void formation [20].

To explain the formation of dust void under different conditions, the researchers proposed various possible mechanisms [10, 17, 18, 21–24]. Among them, Samsonov and Goree proposed that as the particle size grows, unstable modes appear. When the particle size reaches a critical value, the outward ion drag force exceeds the inward electrostatic force, and void appears [21]. Based on the proposed mechanism of void generation, Avinash, Bhattacharjee and Hu established a nonlinear time-dependent self-consistent model (ABH model) for void formation [5]. By adding convection

term to the ABH model under cylindrical coordinate, Liu *et al* proved that the effect of convection term slows down the formation of voids [25]. In [26, 27], a more accurate ion motion equation containing the ionization term is considered. In [27], it is shown that if the ionization rate is larger than a threshold, void can evolve in dust cloud. As the ionization rate is further increased, the time required for void formation decreases, the void size first increases, but then decreases. Mishra *et al* explored the relationship between the two non-linear phenomena of void formation and soliton propagation, they also proved that the evolution of void and its decay over time are closely related to ionization parameter [28].

Past studies have shown that in the void, electron density increases, ionization rate increases, and electron temperature decreases, compared to dust clouds [21, 29, 30]. Samsonov and Goree obtained the image of electron temperature through particle spectral lines in dusty plasma, and found that the electron density/temperature in the circular void region is higher/lower than that in the dust cloud, which is consistent with dust particles dissipating electrons and reducing electron density in the dust cloud [30]. Zhang *et al* studied the radial distribution of electron density and electron temperature in plasma at different frequencies and found that electron temperature is unevenly distributed in space [31]. However, in the previous numerical simulation of the void, the electron
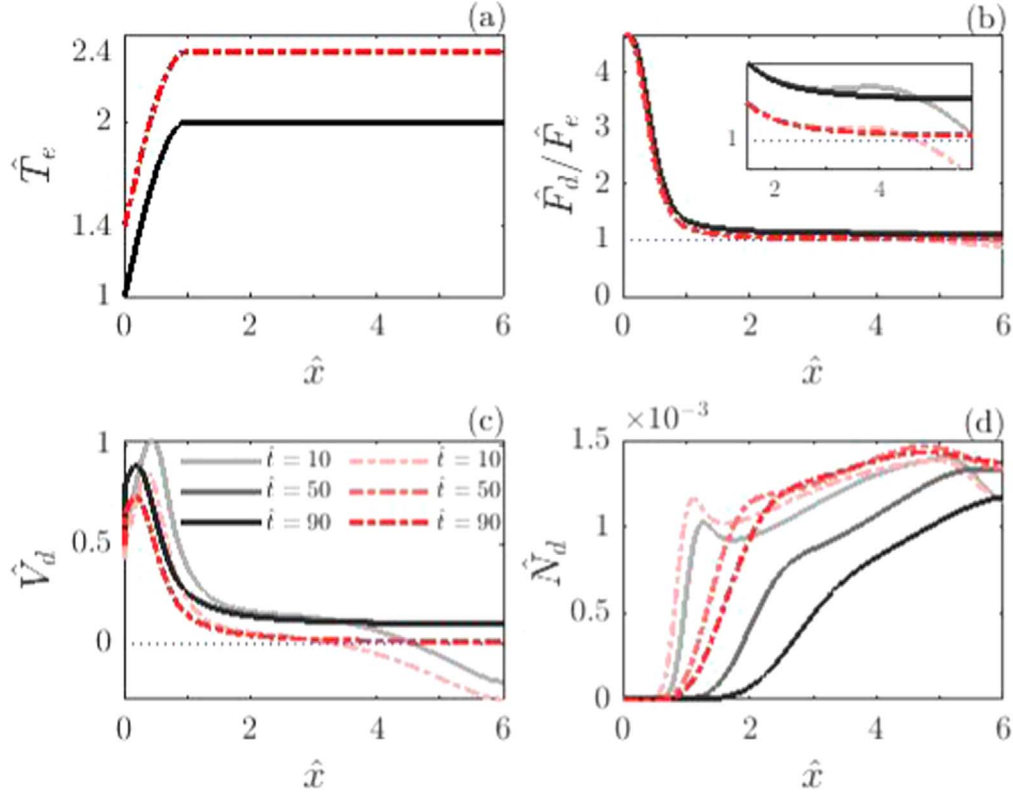
Figure 2. (a) Assumed spatial profiles of electron temperature, corresponding the spatial distribution of (b) the ratio of ion drag force to electrostatic force, (c) dust particle velocity and (d) dust particle number density at $\hat{t} = 10,\ 50$ and 90.

temperature was set as spatially uniform distribution [5, 25–27].

Early research was focused on the generation and evolution of circular void. In addition to the observation of ring void in the experiment, few studies have been done on the mechanism of the formation of ring void. Liu *et al* obtained ring void images similar to the experimental results through two-dimensional molecular dynamics simulation [6, 32]. In [33], it is proposed that the influence of dust charge and neutral density on dust void, and that the increase of neutral density leads to the widening of depletion rings and the generation of new ones.

It is known that void formation is a very important process in a dusty plasma system. In dust growth experiment, it can be clearly observed that void phenomena appear in the earlier stage of dust growth [34], which shows the typical fluid characteristics with fast evolution, and eventually stable voids with different structures form. Thus, we will use the fluid model to explore the mechanism of void formation. It was also found that ionization is an important parameter for the generation and evolution of void, and the spatial variations of electron temperature can trigger the change of ionization. Therefore, it is of great significance to explore the effect of electron temperature spatial variations on the generation of void. Combined with previous studies on circular void, in the numerical simulation of this paper, it is considered that the property of ring void is similar to that of circular void, that is, the electron temperature is lower than that of dust cloud. We use the ABH model, which includes

the convection term and the ion momentum equation, assuming the spatial distribution of electron temperature, to simulate the circle void and the ring void, and to analyze the influence of the spatial distribution of electron temperature on the evolution of the circle void and ring void. Based on the simulation results, the cause of the formation of the ring void is speculated in this paper.

2. Model

Our model considers one-dimensional radial axisymmetric dusty plasma based on the ABH model, including the ion continuity equation and ionization effect. Since the time scale of dust motion is much larger than that of ions, it is assumed that on the dust motion scale, ions can quickly respond to a quasi-stable state. According to the typical experimental parameters of plasma discharge, ion density and momentum loss due to ion absorption by the dust particles are negligible [27]. We will consider the one-dimensional geometry for all equations. The continuity equation and the velocity equation of ions can be written as

$$\frac{\partial n_i}{\partial t} + \frac{\partial}{\partial x}(n_i u_i) = K n_e n_n, \tag{1}$$

$$u_i = \frac{eE}{m_i \nu_{in}}, \tag{2}$$

where n_e, n_d, and n_n are the electron, the dust particle and the neutral-particle densities, respectively. m_i and u_i are the ion
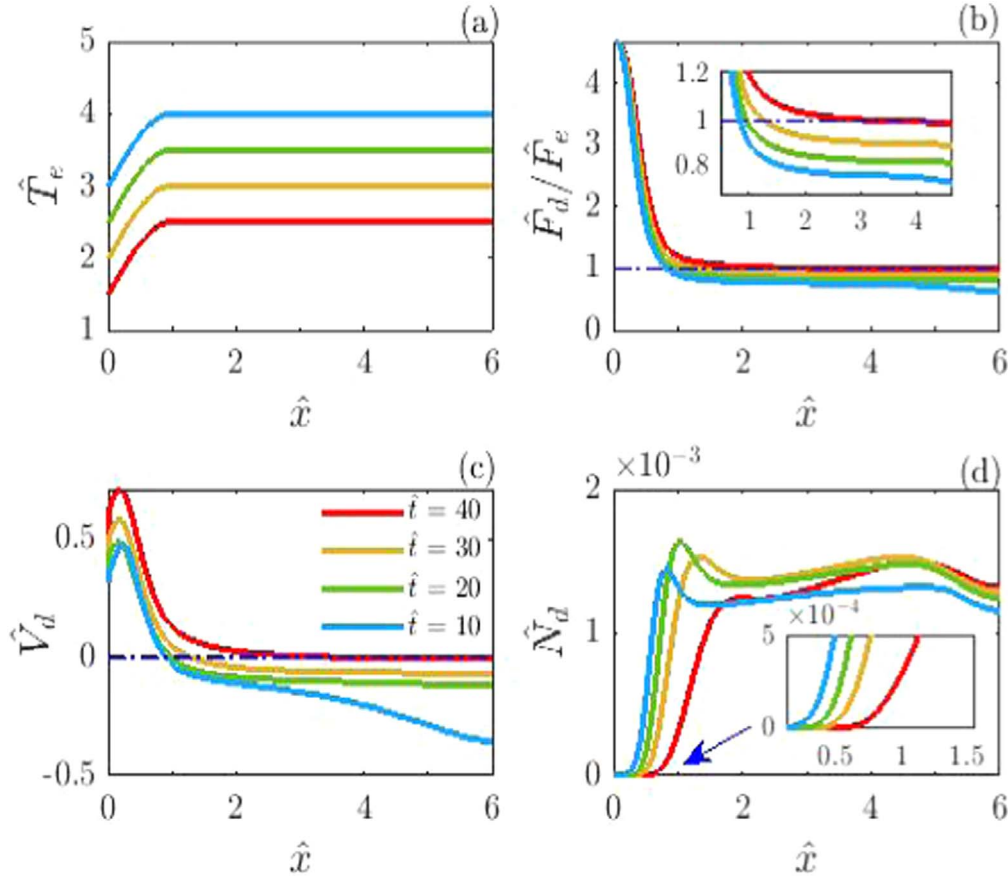
Figure 3. (a) Assumed spatial profiles of electron temperature. When steady state is reached, corresponding the spatial distribution of (b) the ratio of ion drag force to electrostatic force, (c) dust particle velocity and (d) dust particle number density. The $\hat{t}$ in the figure 3(c) is the time to reach steady state.

mass and velocity, respectively, K is the ionization rate, and ν_{in} is the ion-neutral collision frequency.

When the dusty plasma is disturbed, the inertia term of the electron can be neglected due to its lighter mass. The disturbance of the electron can be considered as instantaneous equilibrium. In equilibrium, the resultant net force from the electrostatic effect and the pressure on the electron is zero, and the force balance equation can be expressed as

$$eE + \frac{T_e}{n_e}\frac{\partial}{\partial x}n_e = 0, \tag{3}$$

where T_e is the electron temperature and E is the electric field.

Considering that dust particles are subjected to the electrostatic, the ion drag, the neutral gas frictional and the pressure forces, the dust particle continuity equation and momentum equation can be written as [5]

$$\frac{\partial n_d}{\partial t} + \frac{\partial}{\partial x}(n_d u_d) = D\frac{\partial^2}{\partial x^2}n_d, \tag{4}$$

$$m_d\left(\frac{\partial \boldsymbol{u}_d}{\partial t} + u_d\frac{\partial}{\partial x}u_d\right) = -ZeE$$
$$+ F_d - \nu_{dn}m_d u_d - \frac{T_d}{n_d}\frac{\partial}{\partial x}n_d, \tag{5}$$

where $-Ze$, u_d, m_d, and T_d are the charge, velocity, mass and

temperature of the dust particles, respectively. D is the diffusion coefficient of dust particle. ν_{dn} is dust-neutral collision frequency. In this model, the ion drag force is given by $F_d = m_d \nu_{di} u_{thi} u/(b + u^3)$, with $u = u_i/u_{thi}$, where $u_{thi} = \sqrt{T_i/m_i}$ is ion thermal velocity, and ν_{di} is ion-dust collision frequency, b is a positive constant [5]. These equations are completed by Maxwell's equation,

$$\frac{\partial}{\partial x}(\varepsilon E) = e(n_i - n_e - Zn_d). \tag{6}$$

Introducing dimensionless variables: $Zn_d/\varepsilon n_i \rightarrow \hat{n}_d$, $n_e/\varepsilon n_i \rightarrow \hat{n}_e$, $u_i/u_{thi} \rightarrow \hat{u}_i$, $u_d\tau_i/(\lambda_{Di}\omega_{pd}) \rightarrow \hat{u}_d$, $Ee\lambda_{Di}/T_e \rightarrow \hat{E}$, $x\tau_i/\lambda_{Di} \rightarrow \hat{x}$, $t\omega_{pd} \rightarrow \hat{t}$, $F_d\tau_i/m_d\lambda_{Di}\omega_{pd}^2 \rightarrow \hat{F}_d$, $T_e/T_{e0} \rightarrow \hat{T}_e$, where, $\tau_{i(d)} = T_{i(d)}/T_e$, $\lambda_{Di} = \sqrt{T_i/(4\pi n_i e^2)}$, $\omega_{pd} = \sqrt{4\pi n_{d0}Z^2 e^2/m_d}$, $\omega_{pi} = \sqrt{4\pi n_i e^2/m_i}$, $G = Kn_n/(\tau_i\omega_{pi})$, $T_{e0} = 1$ eV. Equations (1)–(6) can thus be transformed as

$$\frac{1}{\hat{n}_e}\frac{\partial \hat{n}_e}{\partial \hat{x}} = -\frac{\hat{E}}{\tau_i}, \tag{7}$$

$$\hat{u}_i = \mu\hat{E}, \tag{8}$$

$$\frac{\partial \hat{n}_i}{\partial \hat{t}} + \frac{1}{\hat{x}}\frac{\partial(\hat{x}\hat{n}_i\hat{u}_i)}{\partial \hat{x}} = G\hat{n}_e, \tag{9}$$
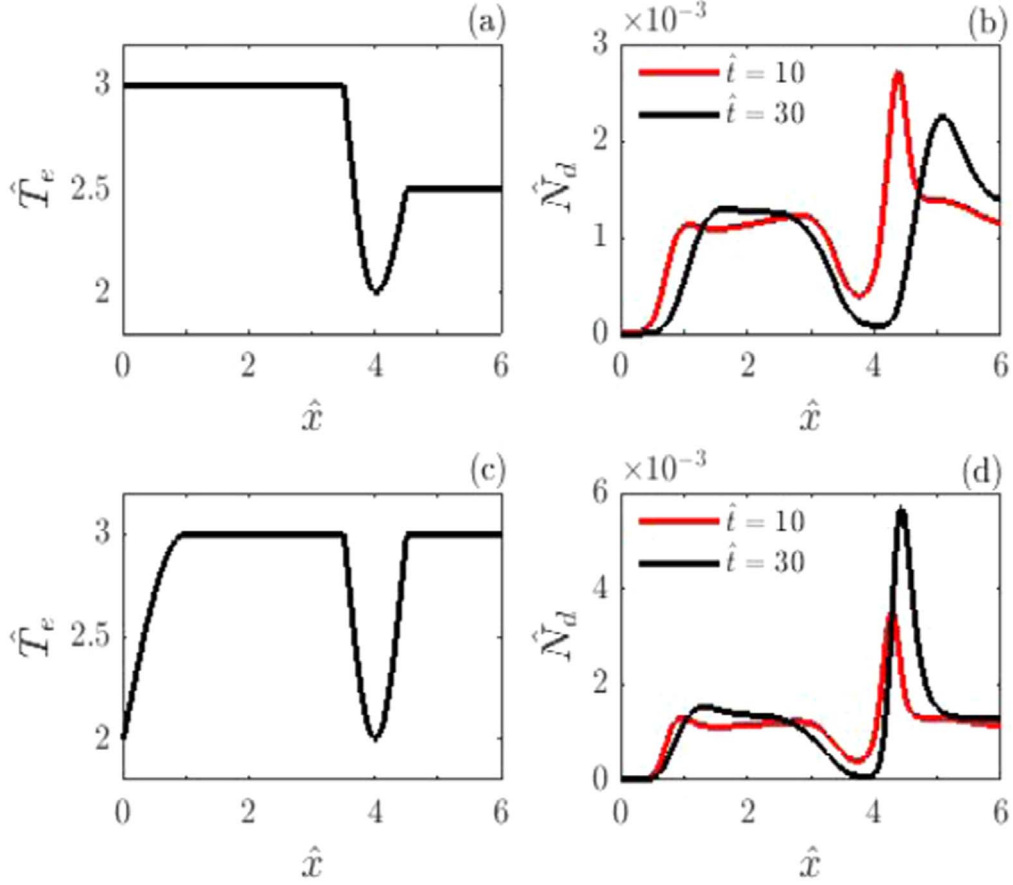
Figure 4. Assumed spatial profiles of electron temperature given in (a) and (c). The corresponding spatial distribution of dust particle number density at $\hat{t} = 10$ and 30 given in (b) and (d).
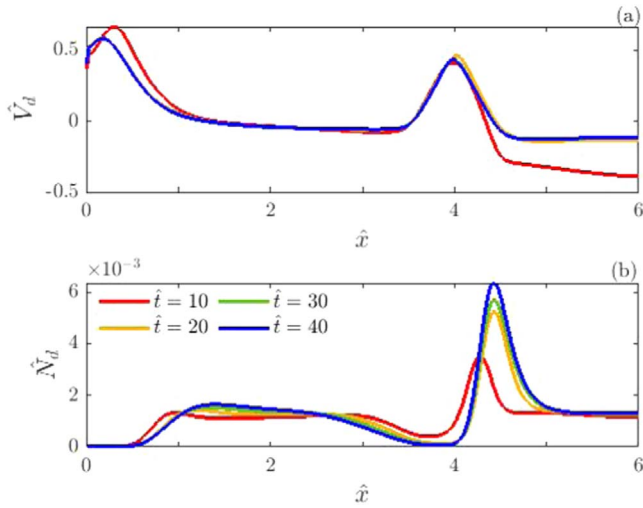

Figure 5. The spatial distribution of (a) dust particle velocity and (b) number density at $\hat{t} = 10,\ 20,\ 30$ and 40. The results correspond to the spatial profile of electron temperature given in figure 4(c).

$$\frac{\partial \hat{n}_d}{\partial \hat{t}} + \frac{1}{\hat{x}}\frac{\partial(\hat{x}\hat{n}_d\hat{u}_d)}{\partial \hat{x}} = D_0 \frac{1}{\hat{x}}\frac{\partial}{\partial \hat{x}}\left(\hat{x}\frac{\partial \hat{n}_d}{\partial \hat{x}}\right), \quad (10)$$

$$\frac{\partial \hat{u}_d}{\partial \hat{t}} + \hat{u}_d \frac{\partial \hat{u}_d}{\partial \hat{x}} = \frac{a\hat{E}}{b + |\hat{u}_i|^3} - \hat{E} - \alpha_0 \hat{u}_d - \frac{\delta}{\hat{n}_d}\frac{\partial \hat{n}_d}{\partial \hat{x}}, \quad (11)$$

$$\frac{1}{\hat{x}}\frac{\partial(\hat{x}\hat{E})}{\partial \hat{x}} = 1 - \hat{n}_e - \hat{n}_d, \quad (12)$$

where $\alpha_0 = \nu_{dn}/\omega_{pd}$, $D_0 = D\tau_i^2 \omega_{pd}/\lambda_{Di}^2$, $\delta = \tau_d/Z$, $\mu = \omega_{pi}/(\nu_{in}\tau_i)$, $a = m_d v_{di}/(m_i Z v_{in})$.

3. Results

The second-order finite difference scheme was utilized in both time and space to solve these equations, with the integration steps being $\Delta\hat{x} = 0.01$ and $\Delta\hat{t} = 0.0001$. We integrated equations (7)–(12) in the range of $0 \leqslant \hat{x} \leqslant 6$. According to the typical experimental parameters we set $\omega_{pd} \approx 406\ \text{s}^{-1}$, $\lambda_{Di} = 0.0052\ \text{cm}$ [25–27, 35]. We adopted the relevant parameters $\alpha_0 = 2.0$, $a = 7.5$, $b = 1.6$, $\delta = 0.001$ and $D_0 = 0.01$ [5, 25–28]. Different from the previous simulations, in this paper we set up the non-uniform distribution of electron temperature in space. And the relevant parameters change to $\tau_i = 0.375/\hat{T}_e$, $\tau_d = 0.003/\hat{T}_e$, $\mu = 0.1875/\tau_i$. The initial conditions are set as $\hat{n}_d = 0.001$, $\hat{n}_e = 0.999$, $\hat{u}_d = 0$, $\hat{E} = 0$. Due to the symmetry around $\hat{x} = 0$, we have $\hat{u}_d = 0$, $\hat{E} = 0$, and $\partial\hat{n}_d/\partial\hat{x} = 0$ at all $\hat{t}$. We use open boundary conditions at $\hat{x} = 6$, i.e., $\partial\hat{n}_d/\partial\hat{x} = 0$ and $\partial\hat{u}_d/\partial\hat{x} = 0$ at all $\hat{t}$.
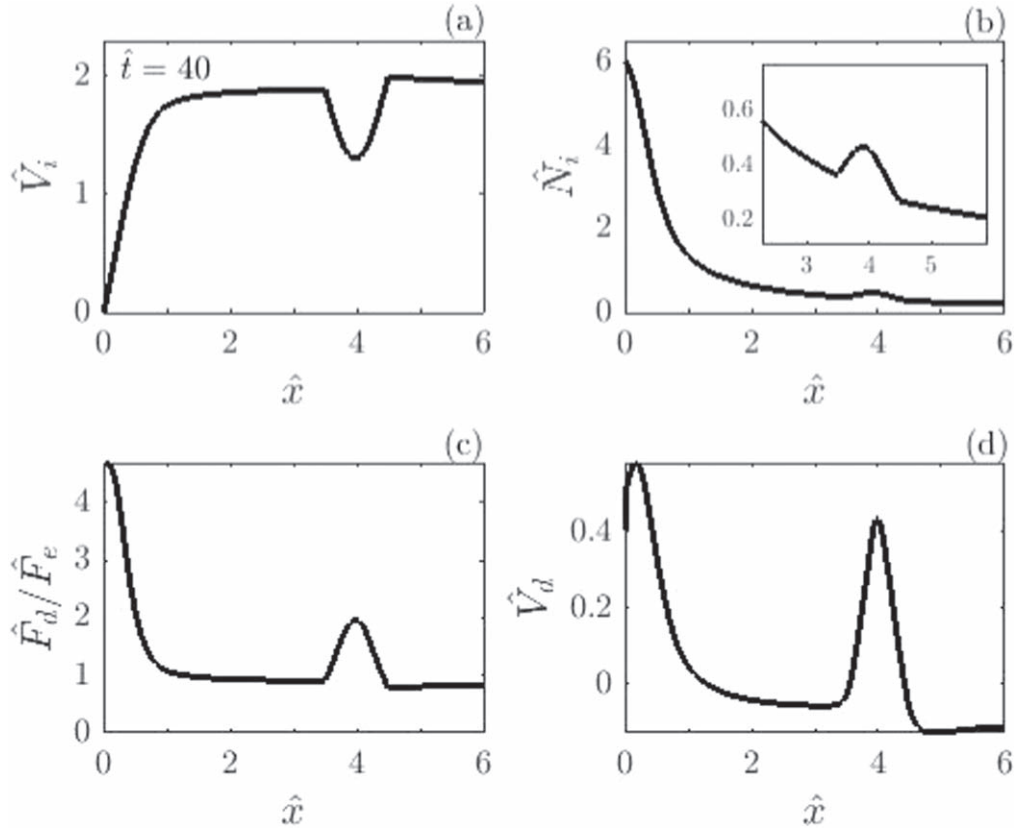
Figure 6. The spatial distribution of (a) ion velocity, (b) ion number density, (c) the ratio of ion drag force to electrostatic force and (d) dust particle velocity in steady state ($\hat{t} = 40$). The results correspond to the spatial profile of electron temperature in figure 4(c).

Figure 1 shows the spatial distribution of the ratio of ion drag force to electrostatic force, the dust particles velocity and number density when the electron temperature is uniformly distributed in space. The black lines in figures 1(a) and (b) show that when $\hat{T}_e = 2$, the outward ion drag force is greater than the inward electrostatic force in space, and the dust particles always flow out. In figure 1(c), curves $1 - 5$ successively represent the spatial distribution of dust particle number density when $\hat{T}_e = 2$ and $\hat{t} = 10$, 30, 50, 70 and 90, indicating that no stable circular void is generated. With the increase of electron temperature, when the electron temperature is higher than the critical value ($\hat{T}_e = 2.9$), a stable circular void can be formed. The color lines (excluding black) in figures 1(a), (b) and (d) represent the spatial distribution of these parameters when steady state is reached at different electron temperatures. Figure 1(a) shows the time when the void reaches steady state at different electron temperatures. It can be seen that the ratio of ion drag force to electrostatic force decreases with the increase of electron temperature. Where $\hat{F}_d = \hat{F}_e$ and $\hat{V}_d = 0$ appear. Therefore, a stable circular void can be generated, and as the electron temperature increases, the time required to reach steady state and circular void size decreases. No ring void is observed when the electron temperature is uniformly distributed.

In the past simulations, the electron temperature was set to a uniform spatial distribution [5, 25–27]. However, based on the measurement of the electron temperature in the void and the dust cloud, it is found that the electron temperature in the void is lower than that in the dust cloud [30]. Therefore, we assume that the spatial distribution of electron temperature is in the form of figures 2(a) and 3(a), with $\hat{x} = 1$ as the dividing line, the electron temperature is uniformly distributed in the region of $\hat{x} > 1$. Figure 2 shows that when the electron temperature is less than the threshold (here is expressed as the red line ($\hat{T}_e(\hat{x} = 0) = 1.4$, $\hat{T}_e(\hat{x} > 1) = 2.4$) in the figure 2(a)), the ion drag force is greater than the electrostatic force in space, dust particles always flow outward, no stable circular void. In figure 3, the spatial distribution of electron temperature is larger than the threshold value. With the increase of electron temperature, the positions of $\hat{F}_d = \hat{F}_e$ and $\hat{V}_d = 0$ appear when reaching the steady state, that is, the circular void has a stable boundary. Figure 3(c) shows the time to reach steady state at different temperatures, decreasing with temperature rise. In figure 3(d), the boundary position of the steady-state void is in the region of $\hat{x} < 1$, which is also in accordance with results that the electron temperature in the void is lower than that in the dust cloud. At the same time, with the increase of the electron temperature, the size of the circular void decreases. Combined with figures 1–3, it is found that the setting of electron temperature in the central region has no effect on the study of the evolution law of the circular void, both of them have the same evolution law, but no ring void is observed.

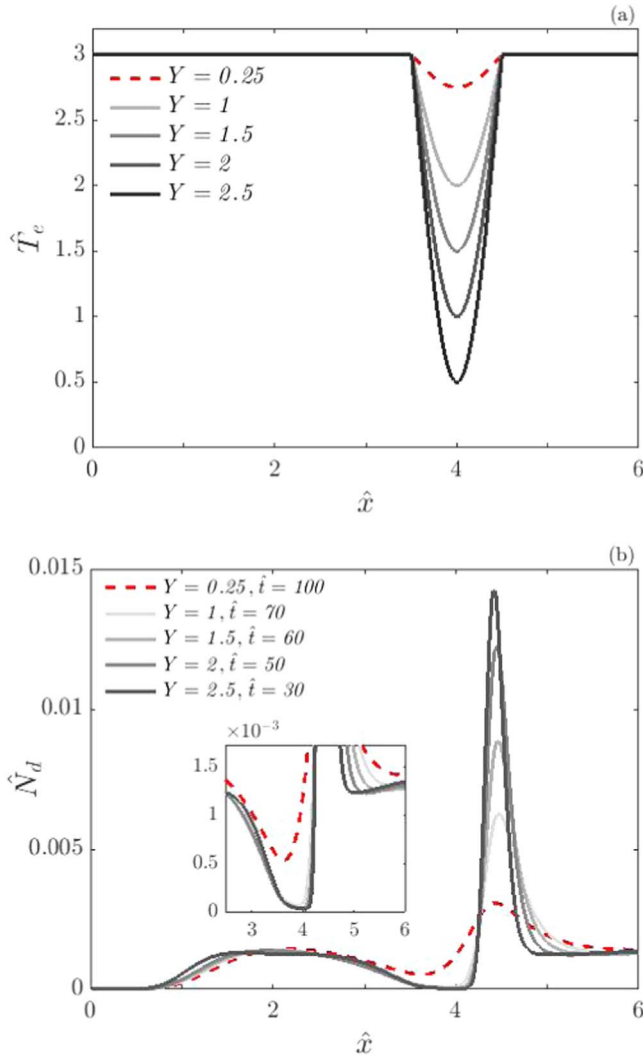Combined with the study of electron temperature, electron density and ionization rate in the circular void

Figure 8. The normalized size of the ring void (when the steady state is reached) as a function of Y. The area with $\hat{N}_d < 10^{-4}$ is considered as a void.

Figure 7. (a) Assumed spatial profiles of electron temperature. The parameter Y indicates the intensity of the spatial variations of the electron temperature. (b) The corresponding spatial distribution of dust particle number density in steady state. The value of $\hat{t}$ given in the figure 7(b) is the time to reach steady state.

[21, 29, 30], and the electron temperature increases with the increase of dust density [24], we propose that the changes of these parameters in the ring void may be consistent with the circular void, that is, the electron temperature in the ring void is also lower than that in the dust cloud. Based on this conjecture, we hypothesize different spatial distribution of electron temperature, and study the influence of spatial variations intensity of electron temperature on the ring void. It is found that when the electron temperature spatial variations are set, the ring void can be obtained by simulation. By changing the setting of electron temperature, the change of the time required to reach steady state and size of the ring void is obtained.

Based on the conjecture of the electron temperature at the ring void, we assume that the radial distribution of the electron temperature is shown in figures 4(a) and (c), and we focus on the spatial variations of the electron temperature in the region of $3.5 < \hat{x} < 4.5$. Figures 4(b) and (d) show the
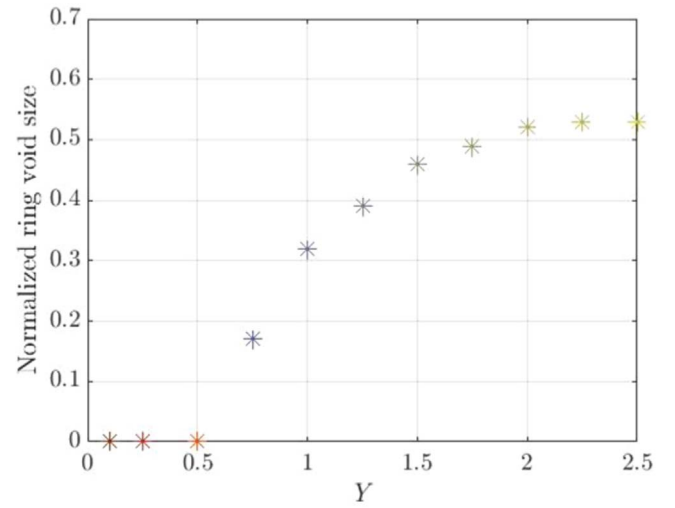
spatial distribution of the dust particle density when $\hat{t} = 10$ and $\hat{t} = 30$, respectively, corresponding to the electron temperature in figures 4(a) and (c). It is found that $\hat{N}_d \to 0$ appears first in the center when $\hat{t} = 10$, that is, the circular void is generated before the ring void, which is consistent with the result observed in the experiment in [3, 4]. When $\hat{t} = 30$, a clear ring void is observed, and the position of the ring void is consistent with the spatial variations of the electron temperature.

Figure 5 shows the spatial distribution of dust particle velocity and number density at $\hat{t} = 10$, 20, 30and 40 under the spatial distribution of electron temperature in figure 4(c). Figure 5(a) shows that because in the region around $\hat{x} = 4$ (the region where the electron temperature changes in space) the dust particles have a velocity greater than that in the dust cloud, the dust particles are expelled faster, and the ring void is generated in this region. At $\hat{t} = 40$, the ring void has been generated and tends to be stable. At this time, $\hat{V}_d \to 0$ is in the region of $1 < \hat{x} < 3.55$ and $\hat{x} > 4.4$. The range of this region is related to the setting of the initial electron temperature spatial variations. Figure 6 shows corresponding to the spatial distribution of the electron temperature in figure 4(c), the spatial distribution of ion velocity, ion number density, the ratio of ion drag force to electrostatic force and dust particle velocity in steady state ($\hat{t} = 40$). It can be seen that in the region near $\hat{x} = 4$, the ion velocity decreases, the ions gather, the ion number density increases, and the resultant force of the ion drag force and electrostatic force on the dust particles increases, the dust particle velocity increases, so the ring void is generated.

To explore the effect of the spatial variations of the electron temperature on the time required to reach steady state and size of the ring void, we assume that the electron temperature distribution in the shape shown in figure 7(a), set the uniform distribution ($\hat{T}_e = 3$) in the region of $\hat{x} < 3.5$ and $\hat{x} > 4.5$, and set the distribution profile as
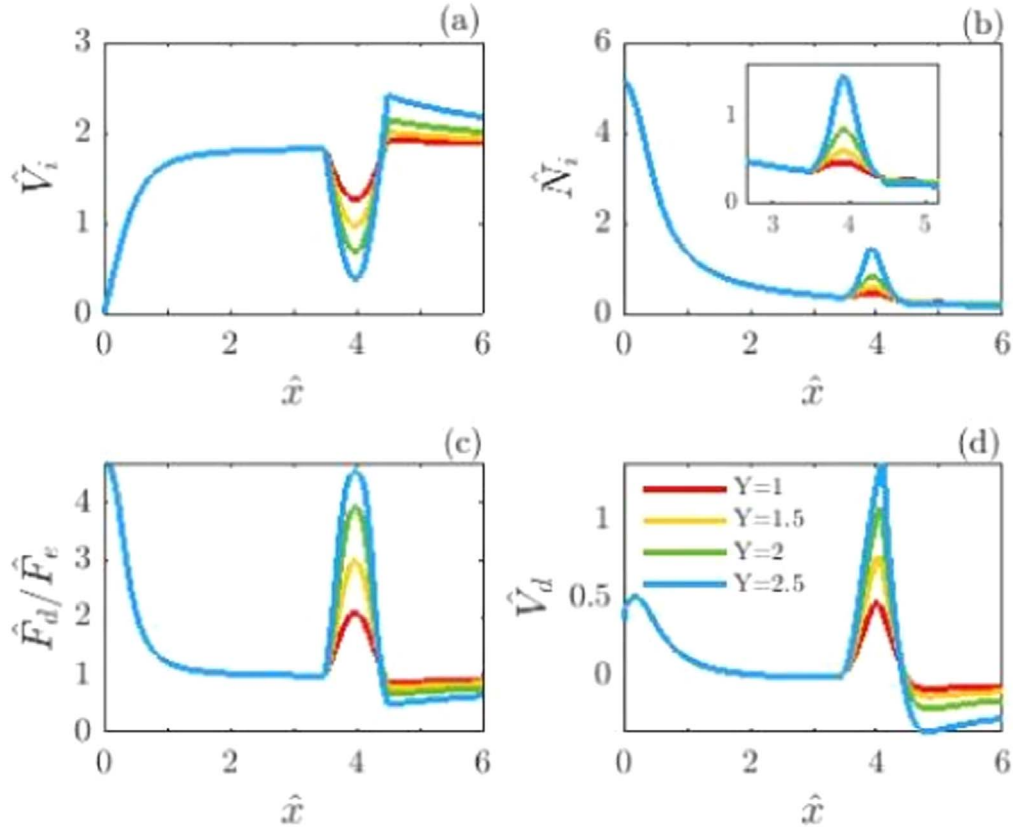
Figure 9. The spatial distribution of (a) ion velocity, (b) ion number density, (c) the ratio of ion drag force to electrostatic force and (d) dust particle velocity at steady state. The results were based on the spatial profiles of electron temperature given in the form of figure 7(a), corresponding to different Y.
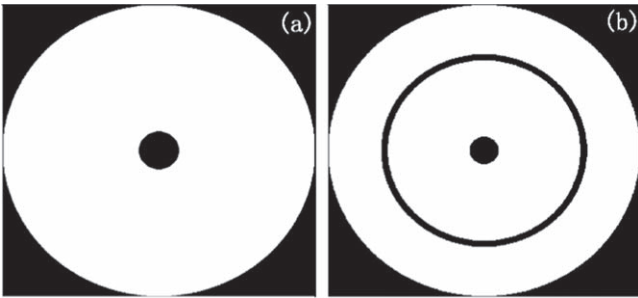

Figure 10. (a)–(b) The simulated circular void and ring void, the area with $\hat{N}_d < 10^{-4}$ is set to black.

$\hat{T}_e = Y^* \sin(\pi^*(\hat{x} + 0.5)) + 3$ in the region of $3.5 < \hat{x} < 4.5$. The parameter Y indicates the intensity of the spatial variations of the electron temperature, and the larger the value of Y represents the more intense the spatial variations of the electron temperature. Figure 7(b) shows the spatial distribution of dust particle number density when steady state is reached at different values of Y, and the time to steady state is given. With the value of Y increases, the time to reach steady state decreases. Figure 8 shows the normalized size of the ring void when the steady state is reached at different the values of Y, and the area with $\hat{N}_d < 10^{-4}$ is set as the void. Combining

figure 7(b) and 8, it can be seen that when $Y < 0.75$, no ring void is generated. When $Y > 0.75$, the size of the ring void increases slightly as Y increases, and approximately remains unchanged when $Y > 2$.

Figure 9 shows the spatial distribution of ion velocity, ion number density, ratio of ion drag force to electrostatic force and dust particle velocity at steady state, corresponding to different values of Y. It can be seen that the larger the Y is, the lower the corresponding electron temperature is, the more intense the spatial variation of the electron temperature is, the smaller the ion velocity is, the higher the number density of the ions is, the greater the resultant force on the dust particles is, the faster the dust particles move, the faster the particles are expelled, and the less time it takes to produce the ring void. In figure 9(c), by observing the positions of $\hat{F}_d = \hat{F}_e$ corresponding to different values of Y, it is found that the positions are similar to each other, and the positions corresponding to the boundary of the ring void are similar to each other. The size of the ring void changes slightly, which is consistent with the conclusion the experiment in [3, 4].

Figure 10 shows that the simulation results are converted into grayscale, the area with $\hat{N}_d < 10^{-4}$ is set to black. We can clearly see the circular void and the ring void. Figure 11 presents the images of void observed in the experiment [3]. It can be seen that the degree of fitting is better.
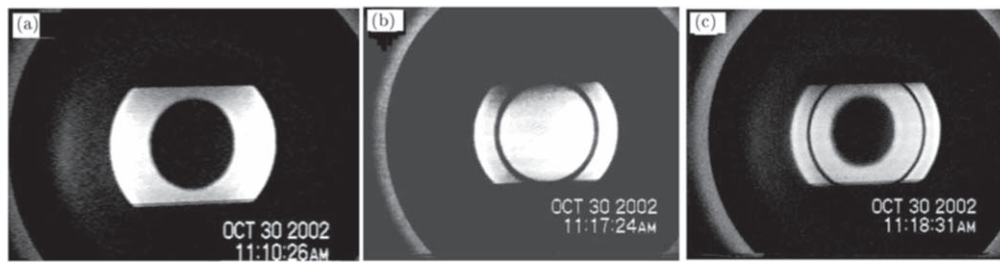
Figure 11. The experimental results (see figure 2 in [3]).

4. Discussion

Based on previous research, it can be known that the electron temperature in the circular void is lower than that in the dust cloud. Different from previous numerical simulations, we assume that the electron temperature spatial distribution is non-uniform. By comparing the simulation results of uniform distribution and non-uniform distribution, it is found that the evolution law of the circular void is the same as the temperature increases in both cases. When the electron temperature is less than the threshold value, no stable circular void is generated. When the electron temperature is greater than the threshold, as the electron temperature rises, the time taken for the circular void to reach a steady state decreases, and the size decreases. In both cases, no ring void appears.

Through the analysis of the circular void, we infer that the electron temperature in the ring void is also lower than that in the dust cloud. By assuming several different non-uniform electron temperature spatial distributions that the electron temperature to change spatially, the images of circular void and ring void are obtained by using computational fluid model, and the circular void is generated before the ring void, which is consistent with the observation in the experiment in [3, 4]. Considering the intensity of the spatial variations of electron temperature, the influence of different strength on ring void evolution is compared. It is found that when the intensity is lower than the threshold, no ring void is generated; when the intensity is higher than the threshold, with the aggravation of electron temperature change in space, the time needed to produce the ring void decreased and the size of the ring void slightly increased.

According to the simulation results, we speculate that the appearance of the ring void may be related to the ion-neutral collisions. The ion-neutral collisions result in the local dissipation of energy [36]. It is possible reason for a drop in electron temperature. The intensity of the collision corresponds to the intensity of the spatial variation of electron temperature in the simulation. When the collision is weak, the spatial variation of electron temperature is weak, and there is no ring void. When the ion-neutral collisions are strong, the resistance of ions increases, resulting in the decrease of ion velocity, the aggregation of ions and the increase of ion drag force, so that the resultant force of ion drag force and electrostatic force on dust particles increases. The velocity of dust particles is faster than that in other dust clouds, and the ring void can be produced. This change is also consistent with the results obtained in the simulation. It is also mentioned that the size of the ring void is related to the average free path of the ion, and it is speculated that the appearance of the ring void is related to the ion-neutral collisions in [4].

5. Conclusion

In summary, based on the ABH model, a one-dimensional fluid model including convection term and explicit ionization is established to study the influence of spatial variations of electron temperature on the formation of void. The images of circular void and ring void are obtained by numerical calculation, and the simulation results are in good agreement with the experimental results in [3, 4]. The present models and results are helpful to understand the generation and development of dust voids in dusty plasma.

References

[1] Shukla P K and Mamun A A 2002 *Introduction to Dusty Plasma Physics* (Bristol: Institute of Physics Publishing) (https://doi.org/10.1088/0741-3335/44/3/701)
[2] Dahiya R P *et al* 2002 Evolution of a dust void in a Radio-Frequency plasma sheath *Phys. Rev. Lett.* **89** 125001
[3] Huang F *et al* 2004 Voids in an experimental dusty plasma system *Chin. Phys. Lett.* **21** 121–4
[4] Huang F *et al* 2004 *Chin. Sci. Bull.* **49** 2150–5
[5] Avinash K, Bhattacharjee A and Hu S 2003 Nonlinear theory of void formation in colloidal plasma *Phys. Rev. Lett.* **90** 075001
[6] Liu Y H, Chen Z Y, Huang F, Yu M Y, Wang L and Bogaerts A 2006 Simulation of disk- and band-like voids in dusty plasma systems *Phys. Plasmas* **13** 052110
[7] Morfill G E *et al* 1999 Condensed plasmas under microgravity *Phys. Rev. Lett.* **83** 1598
[8] Selwyn G S, Heidenreich J E and Haller K L 1990 Particle trapping phenomena in radio frequency plasmas *Appl. Phys. Lett.* **57** 1876
[9] Huang F *et al* 2004 Influence of gas pressure on the pattern evolutions of dust clusters and fractals in a dusty plasma system *Chin. Phys. B* **13** 1896–901
[10] Mamun A A and Shukla P K 2004 Dust voids due to dust-phase-space vortices in plasmas *Phys. Plasmas* **11** 1757

[11] Akdim M R and Goedheer W J 2003 Modeling the effect of dust on the plasma parameters in a dusty argon discharge under microgravity *Phys. Rev. E* **67** 066407

[12] Tribeche M *et al* 2005 Nonlinear plasma void (holes) in a charge-varying dusty plasma *Phys. Plasmas* **12** 092309

[13] Fedoseev A V *et al* 2015 Dust-void formation in a dc glow discharge *Phys. Rev. E* **92** 023106

[14] Tsytovich V N *et al* 2006 Size of dust voids as a function of the power input in dusty plasma *J. Exp. Theor. Phys.* **102** 334–41

[15] Sarkar S, Mondal M, Bose M and Mukherjee S 2015 Observation of external control and formation of a void in cogenerated dusty plasma *Plasma Sources Sci. Technol.* **24** 035007

[16] Shumova V V, Polyakov D N and Vasilyak L M 2017 Influence of dust void on neon DC discharge *Plasma Sources Sci. Technol.* **26** 035011

[17] Vladimirov S V, Tsytovich V N and Morfill G E 2005 Stability of dust voids *Phys. Plasmas* **12** 052117

[18] Zheng X *et al* 2008 The steady structures of dust voids in electronegative plasmas *Phys. Plasmas* **15** 073702

[19] Goree J, Morfill G E, Tsytovich V N and Vladimirov S V 1999 Theory of dust voids in plasmas *Phys. Rev. E* **59** 7055

[20] Tsytovich V N, Vladimirov S V and Morfill G E 2004 Theory of dust and dust-void structures in the presence of the ion diffusion *Phys. Rev. E* **70** 066408

[21] Samsonov D and Goree J 1999 Instabilities in a dusty plasma with ion drag and ionization *Phy. Rev. E* **59** 1047

[22] Jovanović D and Shukla P K 2003 Nonlinear theory for dust voids in plasmas *Phys. Lett. A* **308** 369–74

[23] Khrapak S A, Ivlev A V, Morfill G E and Thomas H M 2002 Ion drag force in complex plasmas *Phys. Rev. E* **66** 046414

[24] Praburam G and Goree J 1996 Experimental observation of very low-frequency macroscopic modes in a dusty plasma *Phys. Plasmas* **3** 1212

[25] Liu Y, Mao S T, Wang Z X and Wang X G 2006 A nonlinear theory of dust voids in cylindrical geometry with the convective effect *Phys. Plasmas* **13** 064502

[26] Liu Y, Wang Z X and Wang X G 2006 Numerical simulation of dust void evolution in complex plasmas with ionization effect *Chin. Phys. Lett.* **23** 3313–5

[27] Hu Z Q *et al* 2009 Theory of void formation in dusty plasmas *Phys. Plasmas* **16** 063707

[28] Mishra R, Adhikari S, Mukherjee R and Dey M 2018 Correlation between two non-linear events in a dusty plasma system *Phys. Plasmas* **25** 123703

[29] Stefanović I *et al* 2008 Plasma density measurements in a developing void *IEEE T. Plasma Sci.* **36** 1018–9

[30] Samsonov D and Goree J 1999 Line ratio imaging of a gas discharge *IEEE Trans. Plasma Sci.* **27** 76–7

[31] Zhang G L *et al* 2019 Experimental investigation of plasma parameters in 13.56 MHz/2 MHz cylindrical inductively coupled plasma *Acta Phys. Sin.* **68** 105202

[32] Liu Y H, Chew L Y and Yu M Y 2008 Self-assembly of complex structures in a two-dimensional system with competing interaction forces *Phys. Rev. E* **78** 066405

[33] Nebbat E and Annou R 2018 Voids in plasmas containing interacting variable charge dust grains *Phys. Plasmas* **25** 093704

[34] Mikikian M *et al* 2017 Optical diagnostics of dusty plasmas during nanoparticle growth *Plasma Phys. Control. Fusion* **59** 014034

[35] Wang X G, Bhattacharjee A, Gou S K and Goree J 2001 Ionization instabilities and resonant acoustic modes *Phys. Plasmas* **8** 5018

[36] Land V and Goedheer W J 2006 *New J. Phys.* **8** 8